Whole-brain activity mapping onto a zebrafish brain atlas

Owen Randlett[1], Caroline L Wee[2], Eva A Naumann[1,8], Onyeka Nnaemeka[1], David Schoppik[1,8], James E Fitzgerald[3], Ruben Portugues[1,8], Alix M B Lacoste[1], Clemens Riegler[1,4], Florian Engert[1,9] & Alexander F Schier[1,3,5–7,9]

In order to localize the neural circuits involved in generating behaviors, it is necessary to assign activity onto anatomical maps of the nervous system. Using brain registration across hundreds of larval zebrafish, we have built an expandable open-source atlas containing molecular labels and definitions of anatomical regions, the Z-Brain. Using this platform and immunohistochemical detection of phosphorylated extracellular signal–regulated kinase (ERK) as a readout of neural activity, we have developed a system to create and contextualize whole-brain maps of stimulus- and behavior-dependent neural activity. This mitogen-activated protein kinase (MAP)-mapping assay is technically simple, and data analysis is completely automated. Because MAP-mapping is performed on freely swimming fish, it is applicable to studies of nearly any stimulus or behavior. Here we demonstrate our high-throughput approach using pharmacological, visual and noxious stimuli, as well as hunting and feeding. The resultant maps outline hundreds of areas associated with behaviors.

The larval zebrafish brain has a size of <0.5 mm^3 and contains ~100,000 neurons. Despite their compact nervous systems and their age of less than 1 week, these animals are capable of a diversity of behaviors. These include swimming in three dimensions, escape maneuvers, visually guided hunting, learning and sleep[1]. To expand our knowledge of how the zebrafish brain is organized functionally and how it produces behavior, we need to identify the neurons and networks relevant to particular tasks. This can begin with measurements of neural activity correlated with behavior. To explore the full range of natural behaviors and to avoid artifacts of manipulation, one should ideally obtain such measurements with freely behaving animals. Calcium-imaging approaches allow nearly brain-wide imaging in larval zebrafish[2,3], but they are limited to head-fixed animals and behaviors that can be performed under a microscope. The recently developed CaMPARI integrative calcium sensor can map activity in freely swimming fish[4], but it requires perturbation through exposure to bright UV light, which causes aversive responses in adult fish[5]. Recording from unperturbed larval zebrafish is possible using aequorin bioluminescent imaging[6], which can provide good temporal resolution, but spatial information is limited to the aequorin expression pattern.

Biochemical events that occur naturally as a consequence of neural activity can be used to identify active neurons in a behaving animal at cellular resolution. In mammals, the expression of immediate early genes (IEGs), such as *c-Fos* and *Arc*, has allowed the localization of neurons critical for diverse behaviors such as memory, sleep, fear, mating and drug addiction[7]. However, the techniques used have relatively poor temporal resolution and suffer from low sensitivity. Indeed, the low amount of baseline c-Fos staining observed in zebrafish brains[8,9] and the relatively slow time course of c-Fos activation of 15–30 min and 1–2 h for mRNA and protein responses, respectively[8,10–14], limit the applicability of *c-Fos* to the study of natural behaviors in zebrafish larvae. Here we used a more permissive endogenous sensor: phosphorylated ERK (also known as MAP)[15–17]. In response to depolarization, calcium influx activates the Ras-ERK pathway[18], leading to the phosphorylation of transcription factors such as CREB and Elk, as well as IEG expression[19]. Therefore, phosphorylated ERK1/2 (pERK) can be used to localize active neurons[12,15,16,20] and offers improved temporal resolution relative to mapping of IEGs, as signals are created within 5 min of activation[15,16,21].

Activity maps are of limited utility unless they intersect with detailed neuroanatomical information[22]. Anatomical resources currently available for larval zebrafish are restricted to maps of fish at 2–4 d post-fertilization (dpf) (ViBE-Z[23]) and two-dimensional images (http://zebrafishbrain.org and ref. 24), from which it can be difficult to infer three-dimensional relationships. Therefore,

[1]Department of Molecular and Cellular Biology, Harvard University, Cambridge, Massachusetts, USA. [2]Program in Neuroscience, Harvard Medical School, Boston, Massachusetts, USA. [3]Center for Brain Science, Harvard University, Cambridge, Massachusetts, USA. [4]Department of Neurobiology, Faculty of Life Sciences, University of Vienna, Vienna, Austria. [5]Broad Institute of MIT and Harvard, Cambridge, Massachusetts, USA. [6]Harvard Stem Cell Institute, Cambridge, Massachusetts, USA. [7]FAS Center for Systems Biology, Harvard University, Cambridge, Massachusetts, USA. [8]Present addresses: Department of Cell and Developmental Biology, University College London, London, UK (E.A.N.); Departments of Otolaryngology and Neuroscience & Physiology, NYU Langone School of Medicine, New York, New York, USA (D.S.); Sensorimotor Control Research Group, Max Planck Institute of Neurobiology, Martinsried, Germany (R.P.). [9]These authors contributed equally to this work. Correspondence should be addressed to O.R. (owen.randlett@gmail.com) or F.E. (florian@mcb.harvard.edu).

RECEIVED 31 MARCH; ACCEPTED 3 AUGUST; PUBLISHED ONLINE 14 SEPTEMBER 2015; DOI:10.1038/NMETH.3581

understanding neuroanatomical features in an activity map is difficult and unstandardized. Here we leveraged high-throughput confocal imaging and registration to create both a reference atlas and brain-wide activity maps.

RESULTS

Z-Brain, a zebrafish reference brain atlas

We chose to create our atlas using zebrafish at 6 dpf, in the often-studied age range of 5–7 dpf. Our goal was to include as many anatomical labels as possible, as well as a detailed segmentation. We registered confocal stacks of the brain to a template brain on the basis of expression of total ERK (tERK) (**Fig. 1**). For registration, we used the Computational Morphometry Toolkit (CMTK)[25,26]. CMTK uses nonrigid registration and morphing algorithms to align imaging data and can achieve an accuracy of 3–4 µm (refs. 26,27). To quantify our registration accuracy, we used spinal backfills to label identifiable reticulospinal neurons in different brains (**Fig. 1b**). Measuring the position of axon emergence from four identified neurons (Mauthner and CaD neurons) yielded a 3D positioning error of approximately one cell-body diameter across registered brains (4.6 µm, mean absolute deviation, n = 23 fish). As the variability in distance between these two neurons in individual fish before warping was 3.2 µm, much of the estimated morphing error might reflect biological variability.

We registered 28 additional labels into the reference brain, for a total of 899 brains (**Supplementary Table 1**). For each label we created a mean-across-fish stack, yielding pseudodensity maps highlighting the domains where labeled components typically reside (**Fig. 1c**,**d** and **Supplementary Video 1**). The accuracy of registration was again evident qualitatively in the overlap of labeled neurons, lamination in the tectal neuropil and a convergence of synaptic markers at the Mauthner axon cap (**Supplementary Fig. 1**). We used these labels, along with Mueller and Wullimann's classical reference atlas[24], to guide the manual segmentation of the reference brain into 294 anatomical regions (**Fig. 1e** and **Supplementary Video 2**).

pERK is a reporter of activity in zebrafish neurons

To determine whether pERK can be used as an activity reporter in larval zebrafish neurons, we stained 6-dpf larvae with anti-pERK. Staining was enriched in the nervous system, and individual cells were evident throughout the brain (**Fig. 2**). In contrast, staining for tERK was more homogeneous, although there was some regional variability in expression. Therefore, we normalized pERK levels to tERK levels (pERK/tERK) for all experiments. To confirm that pERK levels are dependent on neural activity, we optogenetically activated channelrhodopsin 2 (ChR2)-expressing neurons and quantified pERK levels. Blue-light stimulation significantly increased pERK levels in ChR2-expressing

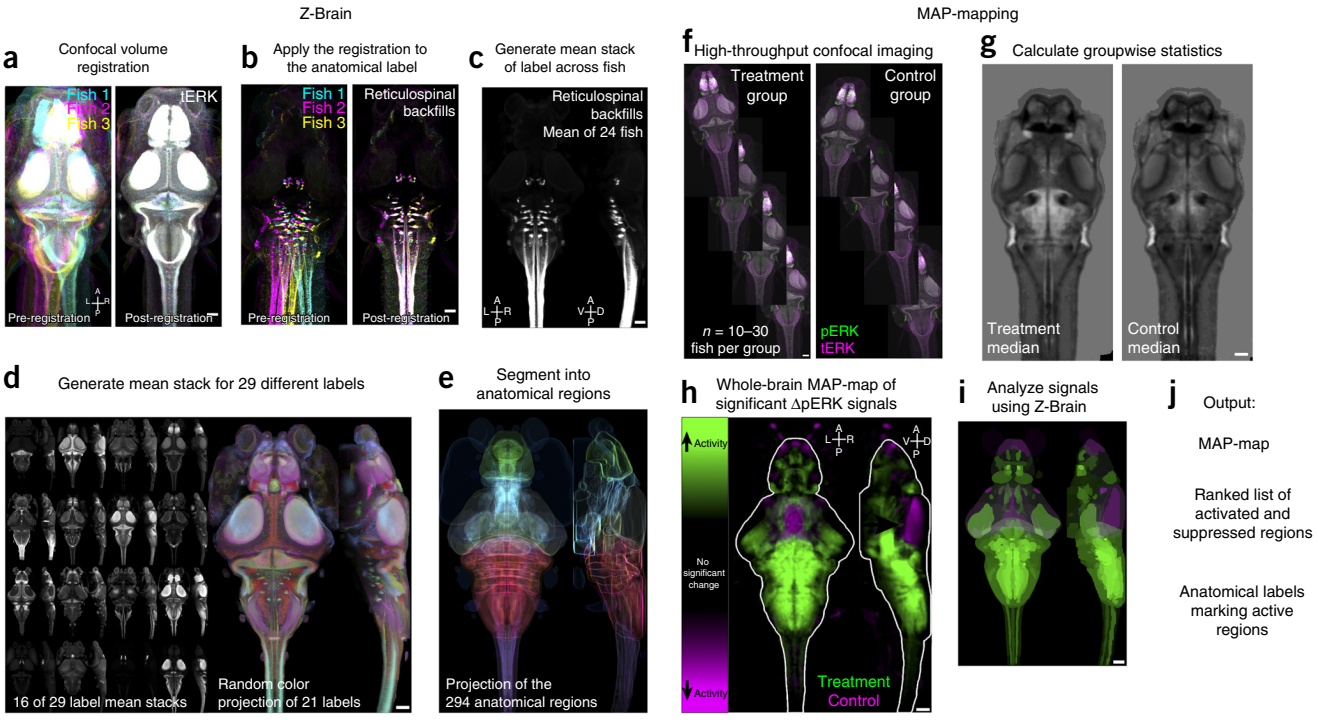

Figure 1 | Analysis pipeline: creating the zebrafish reference brain atlas (Z-Brain) and whole-brain activity maps (MAP-maps). (**a**) Maximum-intensity projections of tERK confocal stacks after registration to a reference brain (n = 3 fish). (**b**) Registrations are applied to an anatomical label (reticulospinal backfills). (**c**) The mean across all registered fish. Shown are Z and X maximum-intensity projections. (**d**) Mean stacks from a total of 29 transgenic, antigenic or dye labels (**Supplementary Table 1**). Shown are maximum-intensity Z and X projections of 16 different labels (left) and Z and X random color projections for 21 labels (right). (**e**) Z and X mean projections of the outlines of the segmented Z-Brain regions (green, telencephalon; cyan, diencephalon; yellow, mesencephalon; red, rhombencephalon; purple, spinal cord). (**f**) For MAP-map creation, pERK and tERK confocal stacks are acquired for ~10–30 fish per condition. (**g**) Stacks are registered to Z-Brain, and the pERK-level statistics are calculated at each voxel. (**h**) Voxels exhibiting significantly higher (green) and lower (magenta) pERK levels in the stimulus group are localized to create a MAP-map (Online Methods). Shown are mean Z and X projections. (**i**,**j**) Analysis of the MAP-map using the Z-Brain (Online Methods). Shown are the Z and X maximum-intensity projections depicting the mean signal in the Z-Brain regions. Scale bars, 50 µm (all panels). R, right; L, left; A, anterior; P, posterior; D, dorsal; V, ventral.

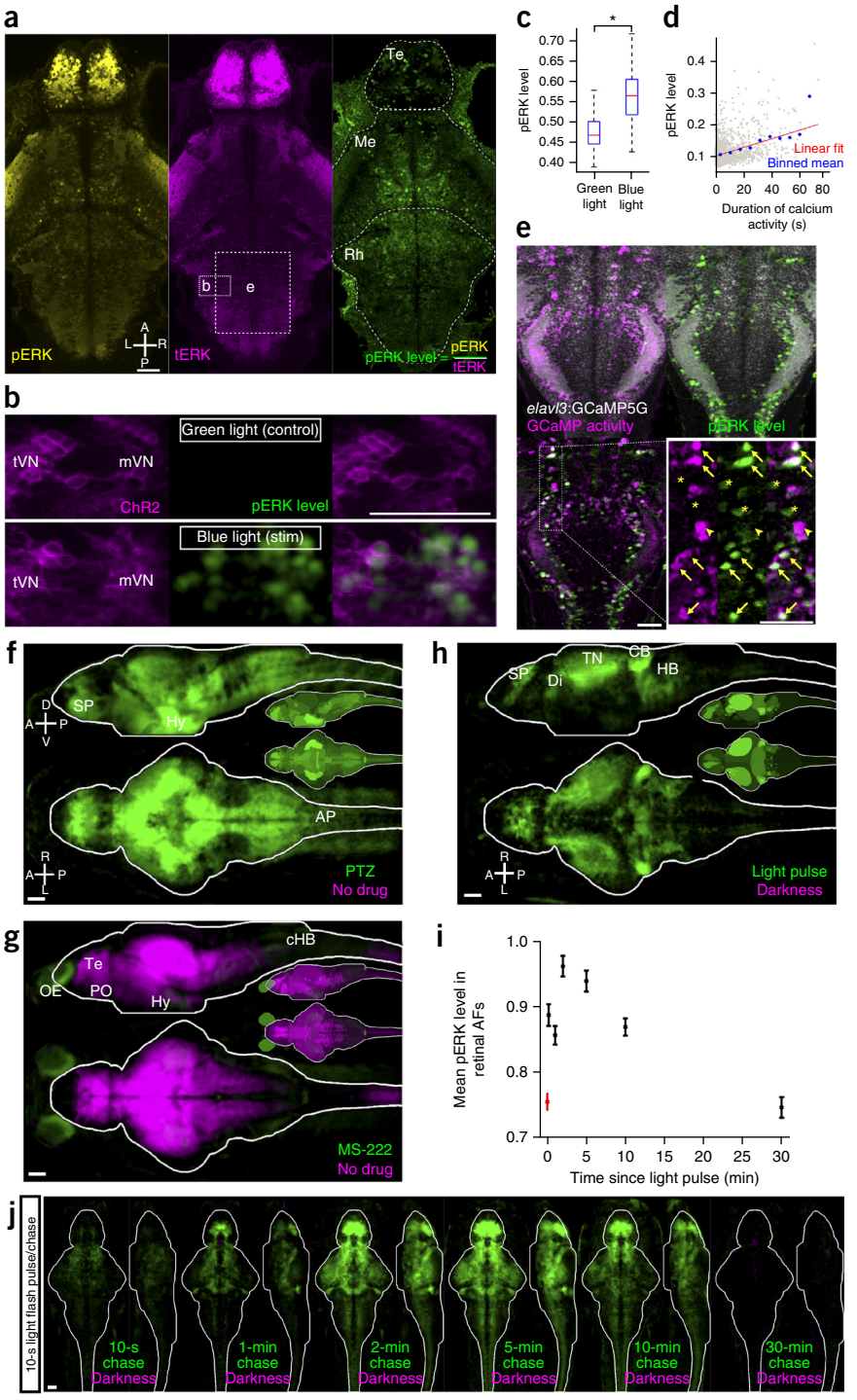

Figure 2 | pERK is a neural-activity marker in zebrafish neurons. (**a**) A confocal slice of a fish stained for pERK (yellow), tERK (magenta) and the normalized pERK level (green). Dashed boxes outline the approximate *x* and *y* positions of neurons shown in **b** and **e**, but in a different *z*-plane. (**b**) ChR2-YFP expression and pERK levels in the tangential and median vestibular nuclei (tVN and mVN) of Tg(−6.7FR*hcrtR*:Gal4VP16); Tg(14x*UAS-E1b*:hChR2(H134R)-EYFP); *atoh7*$^{th241/th241}$; Tg(*atoh7*:GAP-RFP) larvae, stimulated (stim) with either blue or green light. (**c**) pERK levels with and without ChR2 activation (*$P = 8.03 \times 10^{-35}$, Mann-Whitney test; $n = 1{,}056$ neurons from 20 larvae). In the box plots, the red line denotes the median, the blue boxes represent the 25th and 75th quartiles, whiskers extend to the most extreme non-outliers and red crosses mark points considered outliers. (**d**) The total number of seconds an ROI was active during calcium imaging plotted against the pERK level after fixation ($P = 1.1 \times 10^{-66}$, $R = 0.40$, Pearson's correlation; $n = 1{,}771$ ROIs). Plotted are all of the ROIs (gray), the mean in 7-s *x*-bins (blue) and the linear best-fit line (red). (**e**) pERK levels in cells exhibiting calcium activity as identified in correlation analysis (Online Methods and ref. 27). Arrows, asterisks and arrowheads indicate good signal correspondence, potential false positives and false negatives, respectively. (**f**) MAP-map of a zebrafish brain after exposure to 8.25 mM PTZ for 15 min ($n = 12$ each for PTZ and no-drug controls). Insets depict the mean signal in each Z-Brain region in this and other MAP-map panels. (**g**) MAP-map after exposure to 15 mM MS-222 for 1 h ($n = 12$ each for MS-222 and no-drug controls). (**h**) MAP-map of a zebrafish brain after a 10-s light pulse delivered 30 s before fixation ($n = 15$ and $n = 16$ for light-pulse and darkness groups, respectively). (**i**) Mean pERK level (±s.e.m.) in retinal arborization fields (AFs) for dark-adapted larvae (red) and at different chase times after delivery of a 10-s light pulse (black). (**j**) MAP-maps resulting from the experiment described in **i** ($n = 8$ for 10-s pulse, 12 for 2-min pulse, and 13 for 1-min, 5-min, 10-min and 30-min light pulses and for darkness controls). Scale bars, 50 µm (all panels). Te, telencephalon; Me, mesencephalon; Rh, rhombencephalon; SP, subpallium; Di, diencephalon; Hy, hypothalamus; AP, area postrema; PO, preoptic area; OE, olfactory epithelium; cHB, caudal hindbrain; TN, tectal neuropil; CB, cerebellum; HB, hindbrain.

neurons, including neurons in vestibular nuclei (**Fig. 2b**,**c**), habenula, hypothalamus, ventral hindbrain and spinal cord ($P < 2 \times 10^{-5}$ in all cases, Mann-Whitney test; data not shown).

To determine how well pERK reports activity, we performed calcium imaging on fish with pan-neuronal GCaMP5G expression[2], which were stimulated with forward-moving gratings for 15–30 min. Such stimulation activates specific sets of midbrain and hindbrain neurons[28,29]. Fish were then quickly fixed and stained. We re-identified the imaging plane on the basis of the Tg(*elavl3*:GCaMP5G) transgene by morphing the live imaging data into the post-fixation confocal stack (**Supplementary Fig. 2**). The calcium activity of a cell was significantly and consistently correlated with its pERK level (**Fig. 2d**) ($P < 1.5 \times 10^{-12}$, $n = 4$ fish). In a different analysis of the same data, active neurons were highlighted on the basis of the correlation among their pixels[27]. Again, high pERK levels overlapped with active neurons (**Fig. 2e**). However, not all active neurons identified with two-photon calcium imaging showed high pERK levels, hinting at either

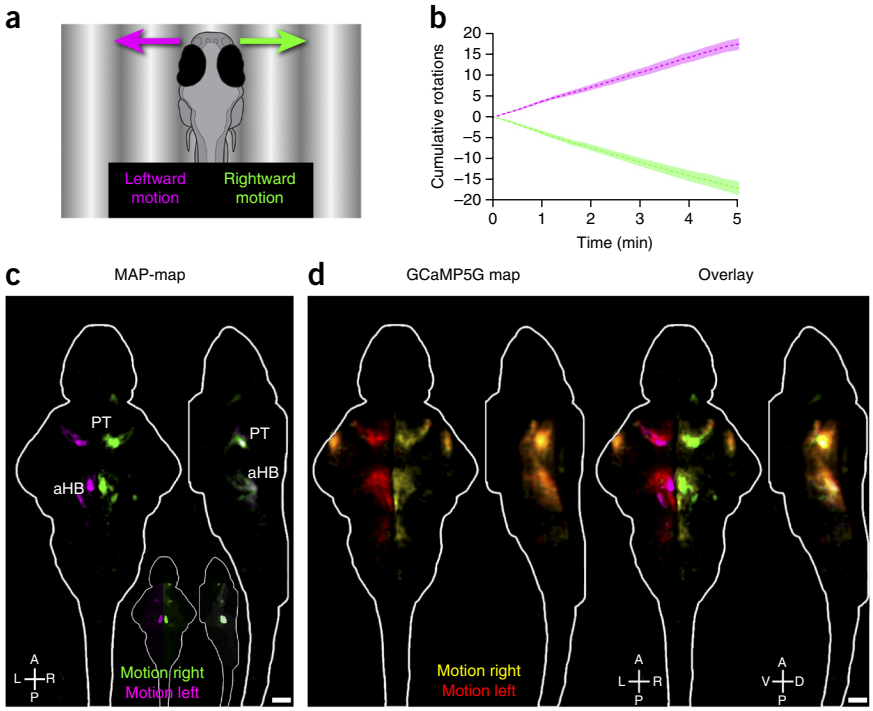

Figure 3 | Neural activity underlying the OMR. (**a**) Larvae were presented with gratings moving to the right (green) or the left (magenta). (**b**) OMR (n = 18 fish per group; dashed lines represent the mean; colored shading extends to ±s.e.m.). (**c**) Differential activity in the fish from **b**. PT, pretectum; aHB, anterior hindbrain. n = 17 and 18 for rightward- and leftward-moving gratings, respectively. (**d**) Two-photon calcium imaging in GCaMP5G-expressing fish stimulated with moving gratings (n = 17). Shown are Z and X projections. Scale bars, 50 µm (all panels).

cell-type differences in pERK activation or a nonlinear relationship between neural activity and pERK staining not revealed by our analysis. Also, some neurons with high pERK levels were not active during calcium imaging. These false positives may reflect neurons that were active outside of the imaging window (for example, signals created during agarose disembedding), neurons whose activity is not detectable by or that do not express GCaMP5G, or perhaps ERK signaling independent of neural activity[30]. We then analyzed the discriminability of pERK for active and inactive cells using the receiver operating characteristic (ROC) (**Supplementary Fig. 3a**,**b**). pERK performed substantially better than a random model, and discriminability of the pERK indicator increased with increasing levels of activity. Finally, we observed strong pERK signals in glutamatergic, GABAergic and glycinergic neurons (**Supplementary Figs. 3c**,**d** and **4**), indicating that none of the major cell classes is refractory to pERK activation. In summary, our findings indicate that pERK levels increase in many active larval zebrafish neurons and can be used as a reporter of activity in this system.

Automated whole-brain neural-activity mapping

High baseline pERK levels make finding stimulus- or behavior-dependent changes in immunostaining challenging. Additionally, potential false positive signals (arising in inactive neurons) necessitate careful comparisons with control samples to ensure that only activity-dependent signals are highlighted. For these reasons, we developed analyses to specifically localize sites of stimulus- or behavior-induced changes in pERK levels (**Fig. 1f**–**h**). Accurate registration of pERK- and tERK-stained brains to the Z-Brain using the tERK stain caused voxels belonging to equivalent physical locations in different fish to overlap. Thus we were able to localize anatomical areas showing differential activity by determining which voxels showed significantly higher or lower pERK levels across treatment and control groups. Using Z-Brain, we were able to then extract active anatomical regions and their corresponding labels from these neural-activity-based MAP-maps (**Fig. 1i**,**j**).

To test whether our approach can be used to identify changes in neural activity, we MAP-mapped fish treated with the $GABA_A$ receptor antagonist pentylenetetrazole (PTZ), which causes strong epileptic activity[6,8,9]. This analysis showed the expected widespread activation (**Fig. 2f**, **Supplementary Video 3** and **Supplementary Data 1**). Next we exposed fish to the sodium channel–blocking anesthetic MS-222 and observed the expected widespread suppression (**Fig. 2g**, **Supplementary Video 4** and **Supplementary Data 1**). This analysis also showed activation in parts of the MS-222–treated brain, suggesting that MS-222 acts as an olfactory stimulant. These control experiments indicated that our approach can identify areas of differential neural activity.

Neural activity underlying visual behaviors

To assess the MAP-mapping approach in behaviorally relevant contexts, we analyzed the response to different visual stimuli. We subjected dark-adapted fish to a 10-s light pulse (**Fig. 2h**, **Supplementary Video 5** and **Supplementary Data 1**) and saw the expected strong signals in the retinal projection fields. Areas of activity were also evident throughout the brain, including in diencephalic areas containing Otpb-labeled neurons, which might reflect signals arising from Opn4a-expressing deep brain photoreceptors[31]. This light-pulse experiment allowed us to perform a pulse-chase experiment to determine the time course of the pERK signal. Consistent with results in rodent neurons[16,21], the signals in zebrafish peaked within 2–5 min of the stimulus and returned to baseline within 30 min (**Fig. 2i**,**j**).

We next analyzed the optomotor response (OMR), which causes fish to follow the direction of whole-field motion. We stimulated freely swimming fish with leftward- or rightward-moving gratings, which induced consistent turning in the direction of the motion (**Fig. 3a**,**b** and refs. 28,29). After 5 min of stimulation and behavioral recording, fish were fixed and MAP-mapped (**Fig. 3c**, **Supplementary Video 6** and **Supplementary Data 1**). When we compared the activity induced by stimulation with rightward-moving versus leftward-moving gratings, we found symmetrical lateralized activity, with the most prominent signals in the pretectum and in two clusters in the anterior hindbrain (aHB) that we referred to as the medial and lateral aHB. For comparison, we performed two-photon calcium imaging on Tg(*elavl3*:GCaMP5G)

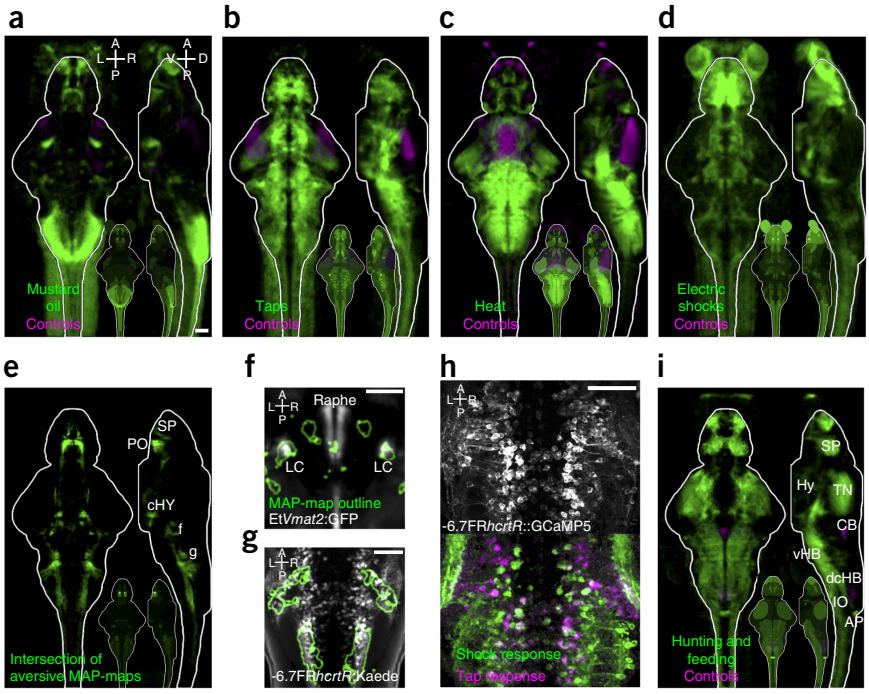

Figure 4 | Activity induced by aversive stimuli and by hunting and feeding. (**a**–**d**) MAP-maps obtained after fish were exposed to aversive stimuli for 15 min: (**a**) 10 µM mustard oil versus DMSO controls (n = 19 and 18 fish, respectively); (**b**) dish taps versus no-tap controls (n = 28 and 29 fish, respectively); (**c**) 37 °C heat versus room temperature (20–23 °C) controls (n = 23 and 21 fish, respectively); and (**d**) electric shocks versus no-shock controls (n = 21 fish for both groups). (**e**) The intersection of the MAP-maps in **a**–**d**. SP, subpallium; PO, preoptic area; cHY, caudal hypothalamic neural cluster. Labels "f" and "g" mark the positions of the structures shown in panels **f** and **g**. (**f**) Z-Brain virtual colocalization of the locus coeruleus (LC) labeled with Et(*Vmat2*:GFP). (**g**) Cells labeled by the Tg(−6.7FR*hcrtR*:Gal4VP16; *UAS*:Kaede) line in the caudal hindbrain. (**h**) Two-photon calcium imaging of Tg(−6.7FR*hcrtR*:Gal4VP16); Tg(*UAS*:GCaMP5G) transgenic larvae stimulated with dish taps and electric shocks. Functional images depict fluorescence correlation with the stimuli. (**i**) MAP-map of the activity induced by 1 h of paramecia exposure, mapped in comparison with a non-fed control group (n = 28 and 23 fish in test and control groups, respectively). TN, tectal neuropil; Hy, hypothalamus; AP, area postrema; SP, subpallium; vHB, ventral hindbrain; IO, inferior olive; CB, cerebellum; dcHB, dorsal-caudal hindbrain. Scale bars, 50 µm.

head-fixed larvae stimulated with leftward- or rightward-moving gratings. Registration of the calcium activity onto Z-Brain showed activation of the same pretectum and aHB regions found by MAP-mapping (**Fig. 3d**), which validated our MAP-mapping results.

The activity in aHB overlapped with GABAergic cells labeled with Tg(*gad1b*:GFP)[32] in Gad1b cluster 1 and Gad1b stripe 1 of the Z-Brain (**Supplementary Fig. 4a**). To follow up, we performed cellular-resolution analysis in Tg(*gad1b*:GFP) larvae stimulated with rightward-moving gratings. On the basis of measured pERK levels, *gad1b*:GFP cells were activated (**Supplementary Fig. 4b**), whereas *gad1b*:GFP-negative neurons in these areas were not as strongly activated. These results describe motion-responsive activity across the brain and identify a new population of hindbrain neurons that may mediate the biased turning behavior induced by whole-field motion.

Neural responses to aversive stimuli

Zebrafish larvae exhibit aversive responses to electric shocks[33], acoustic stimuli such as dish taps[34], the chemical irritant mustard oil and noxious heat[35]. We MAP-mapped the response to a 15-min exposure to each of these stimuli (**Fig. 4a**–**d**, **Supplementary Videos 7**–**10** and **Supplementary Data 1**). As all four stimuli are aversive, we asked whether any regions in the brain are activated or suppressed by all four stimuli (**Fig. 4e**, **Supplementary Video 11** and **Supplementary Data 1**). Areas showing activation by multiple stimuli were present more frequently than would be expected by chance ($P < 1 \times 10^{-15}$, $\chi^2 = 6.4 \times 10^5$), suggesting that a core network is activated by these stimuli. Specifically, all four stimuli led to activation of the locus coeruleus (**Fig. 4f**), a region that regulates arousal and is activated by aversive stimuli in mammals[36]. Activation was also seen in the spinal cord and hindbrain, some of which overlapped with neurons labeled in the Tg(−6.7FR*hcrtR*:Gal4) line[37] (**Fig. 4g**). These are a group of uncharacterized neurons that are likely inhibitory, as they lie in a domain containing mostly GABAergic and glycinergic neurons, according to the Z-Brain database (data not shown). In addition, we performed calcium imaging while delivering tap and shock stimuli (**Fig. 4h**), which confirmed the strong activation of these cells. These experiments isolated activity induced by four aversive stimuli and genetically identified a population of neurons that may mediate general aversion behavior.

Neural activity during hunting and feeding

Prey hunting is one of the remarkable behaviors exhibited by larval zebrafish. Although zebrafish respond to and engage in hunting of small prey-like spots when restrained[38], the complete behavior including capture events and feeding can be studied only in freely swimming larvae. To study hunting- and feeding-dependent activity, we allowed zebrafish to feed on paramecia for 1 h and MAP-mapped their activity relative to that of a nonfed control group (**Fig. 4i**, **Supplementary Video 12** and **Supplementary Data 1**).

Despite the complex nature of this stimulus and behavior, we observed a well-structured activity map. Z-Brain analyses (**Supplementary Fig. 5**) showed activation of the tectal neuropil and the nucMLF MeL/R neurons and surrounding neuropil, which have previously been implicated in prey capture[39]. We observed particularly strong activation of the area postrema, which, to our knowledge, has not been implicated in feeding behavior in zebrafish, although it is a well-known site of feeding regulation in mammals[40]. We also observed suppression in two regions in the dorsal-caudal hindbrain where glycinergic cells reside. The role of this suppressed area remains to be determined, but it serves

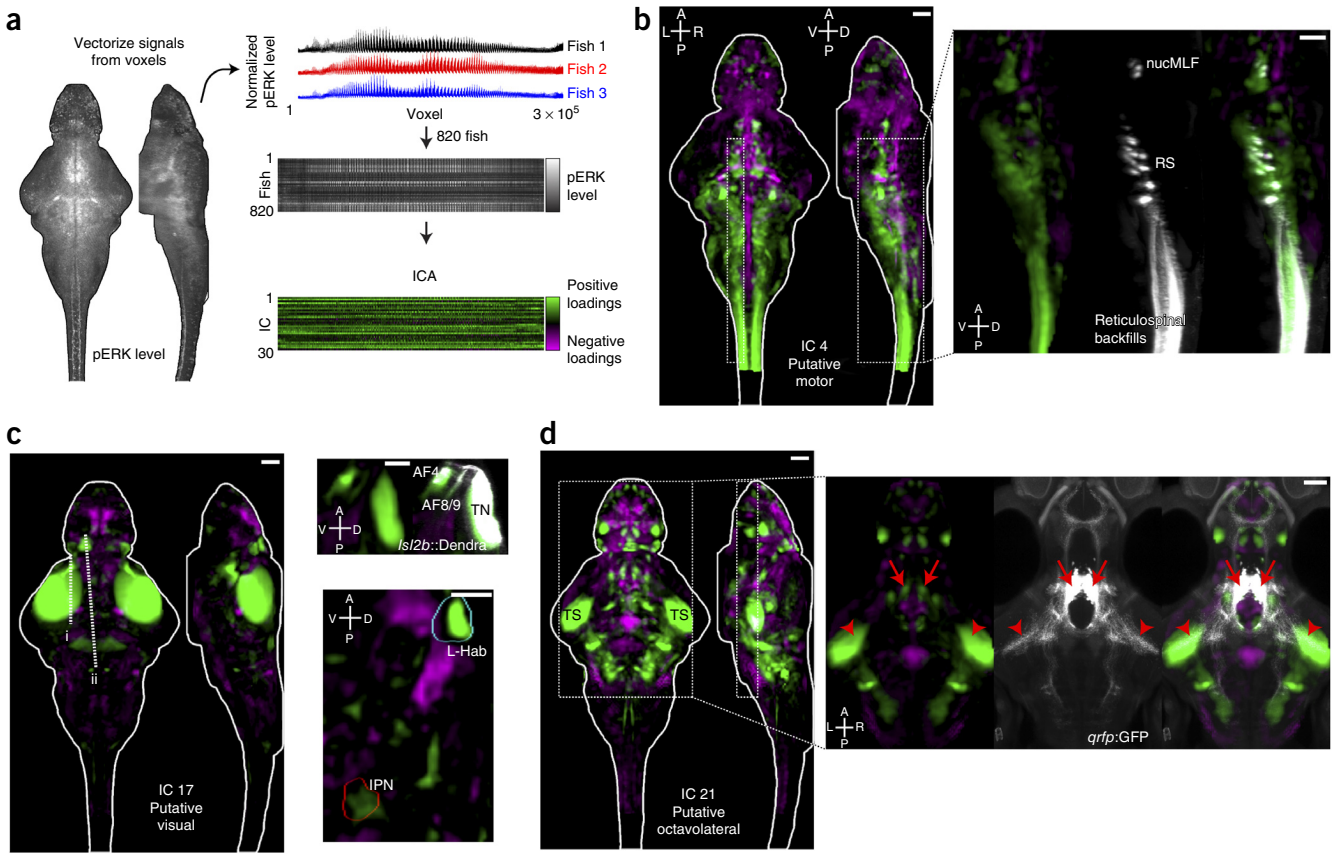

Figure 5 | Spatial ICA across fish as a method for localizing functional brain networks. (**a**) The pERK-level stack was reshaped into a vector, and the vectors from 820 fish were then combined into an array for ICA (Online Methods). (**b**–**d**) Voxels for each recovered IC were painted with their intensity proportional to the *z*-score of the loadings of the ICA signal linearly mapped for $z = 1–4$ and are shown as maximum Z and X projections. (**b**) IC 4 highlights a putative motor network, which associates regions overlapping with reticulospinal neurons (RS), the nucleus of the medial longitudinal fascicle (nucMLF) and the spinal cord. Overlap with the reticulospinal backfill Z-Brain label is shown as an X-projection over the boxed area. (**c**) IC 17 highlights a putative visual-response network. This IC overlaps with areas of retinal arborization fields (AFs) 4, 8 and 9 and the tectal neuropil (TN) labeled by Tg(*Isl2b*:Gal4); Tg(*UAS*:Dendra) in the Z-Brain (right, upper panel). Prominent signals were also observed in the left habenula (L-Hab) and interpeduncular nucleus (IPN) (right, lower panel). Dashed lines in the panel on the left represent the positions of the resliced views in panels on the right. (**d**) IC 21 highlights a putative octavolateral network with prominent signals in the torus semicircularis (TS). Foci of signal in the rostral hypothalamus overlap with the cell bodies of Tg(*qrfp*:GFP)-labeled neurons (right, arrows), which send projections to the TS (arrowheads). Scale bars, 50 µm (all panels).

as an example of the many previously unrecognized areas now implicated in this complex behavior.

Functional association analyses from pERK-stained brains

In total, our experiments provided us with pERK data for 820 fish brains in a variety of pharmacological and behavioral conditions. We wondered whether activity patterns across this array might reveal functional associations among brain regions. Inspired by functional connectivity analyses of functional magnetic resonance imaging and calcium-imaging data sets[41–43], we explored this idea using independent-component analysis (ICA) (**Fig. 5a**). ICA is designed to extract independent signals from linearly mixed observations[44]. In our context, we sought independent brain-wide activity patterns that combined to generate pERK signals. Our analysis yielded anatomically structured maps associating both proximal and distal brain regions (**Supplementary Fig. 6**). Some independent-component (IC) maps recapitulated known anatomical or functional circuitry such as a zebrafish motor network, including the reticulospinal system, nucMLF and spinal cord (**Fig. 5b**). Another IC contained the retinal arborization fields and may represent a visual network (**Fig. 5c**). This IC also contained prominent signals in the left habenula and the interpeduncular nucleus, which are anatomically connected and responsive to light[45,46]. Other ICs could serve as a basis for novel functional associations in the zebrafish brain. For example, we observed associations between specific forebrain and hindbrain nuclei and the midbrain torus semicircularis (**Fig. 5d**), which receives octavolateral (lateral line and acoustic) input in teleosts[24,47]. Close inspection of one nucleus in the rostral hypothalamus showed overlap with Tg(*qrfp*:GFP)-expressing neurons[48]. We found that these neurons sent prominent projections to the torus semicircularis, anatomically validating this functional association between brain areas.

How precisely these ICA maps relate to anatomical and functional circuitry remains unclear, but our results foreshadow how large-scale unsupervised analyses of pERK-stained fish might help to unravel the organizational principles of the zebrafish brain.

DISCUSSION

pERK as a marker of active neurons

pERK is an endogenous sensor that has been used to mark active neurons for more than a decade[15,16], and it can provide improved temporal resolution relative to that obtained with IEGs (**Fig. 2i,j** and refs. 16,21). Historically, pERK has been less widely used as an activity reporter than IEGs because it generally shows higher baseline staining in unstimulated brains. In our experiments, however, this perceived weakness was a major advantage: baseline activity provided an opportunity to find areas that were suppressed relative to control brains.

Although pERK can serve as a useful activity marker, its relationship to activity is complex and dependent on the frequency and repetition of neural firing, and perhaps on cell type[21,49,50]. Thus, the pERK level is not a perfect representation of neural activity. For example, we did not observe OMR-induced activity in the reticulospinal system, although it has been observed with other methods[28,29]. This might indicate that a negative bias exists in detecting activity signals from large-diameter neurons. Although pERK signals might not capture the entire activity pattern in the brain, they are a powerful tool for creating neural-activity maps for freely behaving animals and identifying candidate regions for further analyses.

Using image registration to create activity maps

Our MAP-mapping approach relies on the accurate registration of many brains to a common template to localize changes in activity. Registration-based analyses may work better for some cell types than others, depending on the stereotypy of neuron positioning in different animals. For example, the position of the Mauthner and CaD neurons is precise to within 4 μm, whereas *etVmat2*:GFP-labeled neurons in the medial tectum are much more variably positioned. We found fewer than 20 of these cells randomly distributed within a section of >5,300 μm^2, suggesting that more than 90% of their possible territory is occupied by other cell types. A neuron's positional variability determines over what spatial scale its activity signals are diluted in registration approaches, influencing both signal-to-noise ratio and the resolution of the activity signal. In cases where the position of neurons is highly stereotyped, the resolution can be near-cellular. However, as all of the underlying confocal data used to generate MAP-maps are at cellular resolution, the activated neurons in the MAP-map signal can be identified in individual fish for cellular-resolution analyses.

Interfacing activity and anatomy in a reference atlas

Measuring activity is only the first step toward describing neural circuitry. Next one needs to put the activity in the context of the neuroanatomy, and ideally identify relevant neurons. Using the Z-Brain atlas as our reference brain provides a precise language to describe regions of activity, allows for direct comparisons across experiments, can identify labels for candidate neurons mediating behavior and can reveal brain-wide functional connectivity patterns. Such analyses will become even more powerful as more labels and activity maps are accumulated in the Z-Brain.

Our approach to creating the Z-Brain is conceptually similar to that used for the ViBE-Z atlas[23], but we used a simpler imaging setup and the cross-platform CMTK registration software that can be implemented on a standard computer. Registration quality is accurate to approximately one cell-body diameter and has been validated across species[25–27], different microscopes and even different imaging modalities; we have successfully registered two-photon imaging data into the Z-Brain, allowing us to directly compare MAP-mapping, calcium imaging and anatomical data.

The Z-Brain currently contains 29 labels and 294 segmented regions. Because this many-channel atlas would be cumbersome to visualize using standard visualization software, we built a simple web interface to browse the image data (http://engertlab.fas.harvard.edu/Z-Brain/) and a Matlab-based visualization program that performs multicolor overlays of many channels, rapidly switches between channels and performs click-to-define interrogation of the many anatomical regions (http://engertlab.fas.harvard.edu/Z-Brain/ and https://github.com/owenrandlett/Z-Brain). The Z-Brain is an expandable and editable platform that is open source and freely available. New regional definitions can be easily created, facilitating collaborative input and improvement. As any label of interest can be incorporated into the Z-Brain, the zebrafish community can rapidly expand the atlas by contributing additional anatomical or functional stacks.

In summary, our study presents the Z-Brain atlas and MAP-mapping as a technique for mapping neural activity in freely swimming fish. MAP-mapping has several features that have potential for wide use in characterizing brain regions and neurons that mediate behavior: it is rapid, high throughput and low cost, and it can be performed on freely swimming, unperturbed wild-type larvae, making it applicable for nearly any stimulus or behavior.

METHODS

Methods and any associated references are available in the online version of the paper.

Note: Any Supplementary Information and Source Data files are available in the online version of the paper.

ACKNOWLEDGMENTS

We are grateful to M. Wullimann (Ludwig Maximilian University) for his critical and detailed input regarding the identification of regions for the Z-Brain segmentation, Y. Yoshihara (RIKEN Brain Science Institute) and T. Okuyama (University of Tokyo) for pointing us to the pERK antibody, G. Jefferis (MRC Laboratory of Molecular Biology) for help with brain registrations, M. Nikitchenko (Harvard) for help with computational and web resources, A. Douglass (University of Utah) and J. Wortzman (Harvard) for creation of the Tg(*UAS*:GCaMP5G) line, D. Prober (Caltech) for sharing the Tg(*hcrt*:mRFP) and Tg(*qrfp*:GFP) lines before publication, M. Hasemeyer (Harvard) for many helpful discussions, and the many members of the zebrafish community who shared their transgenic fish lines. Funding was provided by an HFSP Long-Term fellowship (LT000772/2012-L to O.R.); the Agency for Science, Technology and Research, Singapore (C.L.W.); a Marie Curie Fellowship (E.A.N.); the Swartz Foundation (J.E.F.); the Simons Foundation (SCGB award 325207 to F.E.); and NIH grants R01 HL109525, U01 MH105960 (both to A.F.S.), R24 NS086601, U01 NS090449 and DP1 NS082121-02 (to F.E.).

AUTHOR CONTRIBUTIONS

O.R., F.E. and A.F.S. conceived of the project. O.R. performed most experiments and data analysis. C.L.W., E.A.N., D.S. and A.M.B.L. also performed experiments. E.A.N., J.E.F. and R.P. also analyzed data. D.S. and C.R. created new transgenic fish strains. O.N. built the website. O.R., F.E. and A.F.S. wrote the paper, with input from all other authors. F.E. and A.F.S. supervised the project.

COMPETING FINANCIAL INTERESTS

The authors declare no competing financial interests.

1. Fero, K., Yokogawa, T. & Burgess, H.A. The behavioral repertoire of larval zebrafish. in *Neuromethods* Vol. 52 (eds. Kalueff, A.V. & Cachat, J.M.) 249–291 (Humana Press, 2010).
2. Ahrens, M.B., Orger, M.B., Robson, D.N., Li, J.M. & Keller, P.J. Whole-brain functional imaging at cellular resolution using light-sheet microscopy. *Nat. Methods* **10**, 413–420 (2013).
3. Panier, T. *et al.* Fast functional imaging of multiple brain regions in intact zebrafish larvae using selective plane illumination microscopy. *Front. Neural Circuits* **7**, 65 (2013).
4. Fosque, B.F. *et al.* Labeling of active neural circuits *in vivo* with designed calcium integrators. *Science* **347**, 755–760 (2015).
5. Nava, S.S., An, S. & Hamil, T. Visual detection of UV cues by adult zebrafish (*Danio rerio*). *J. Vis.* **11**, 2 (2011).
6. Naumann, E.A., Kampff, A.R., Prober, D.A., Schier, A.F. & Engert, F. Monitoring neural activity with bioluminescence during natural behavior. *Nat. Neurosci.* **13**, 513–520 (2010).
7. Guzowski, J.F. *et al.* Mapping behaviorally relevant neural circuits with immediate-early gene expression. *Curr. Opin. Neurobiol.* **15**, 599–606 (2005).
8. Baraban, S.C., Taylor, M.R., Castro, P.A. & Baier, H. Pentylenetetrazole induced changes in zebrafish behavior, neural activity and *c-fos* expression. *Neuroscience* **131**, 759–768 (2005).
9. Ellis, L.D., Seibert, J. & Soanes, K.H. Distinct models of induced hyperactivity in zebrafish larvae. *Brain Res.* **1449**, 46–59 (2012).
10. Okuyama, T. *et al.* Induction of *c-fos* transcription in the medaka brain (*Oryzias latipes*) in response to mating stimuli. *Biochem. Biophys. Res. Commun.* **404**, 453–457 (2011).
11. Xiu, J. *et al.* Visualizing an emotional valence map in the limbic forebrain by TAI-FISH. *Nat. Neurosci.* **17**, 1552–1559 (2014).
12. Hussain, A. *et al.* High-affinity olfactory receptor for the death-associated odor cadaverine. *Proc. Natl. Acad. Sci. USA* **110**, 19579–19584 (2013).
13. Kovács, K. Measurement of immediate-early gene activation—*c-fos* and beyond. *J. Neuroendocrinol.* **20**, 665–672 (2008).
14. Morgan, J.I., Cohen, D.R., Hempstead, J.L. & Curran, T. Mapping patterns of c-fos expression in the central nervous system after seizure. *Science* **237**, 192–197 (1987).
15. Cancedda, L. *et al.* Patterned vision causes CRE-mediated gene expression in the visual cortex through PKA and ERK. *J. Neurosci.* **23**, 7012–7020 (2003).
16. Ji, R.R., Baba, H., Brenner, G.J. & Woolf, C.J. Nociceptive-specific activation of ERK in spinal neurons contributes to pain hypersensitivity. *Nat. Neurosci.* **2**, 1114–1119 (1999).
17. Xia, Z., Dudek, H., Miranti, C.K. & Greenberg, M.E. Calcium influx via the NMDA receptor induces immediate early gene transcription by a MAP kinase/ERK-dependent mechanism. *J. Neurosci.* **16**, 5425–5436 (1996).
18. Rosen, L.B., Ginty, D.D., Weber, M.J. & Greenberg, M.E. Membrane depolarization and calcium influx stimulate MEK and MAP kinase via activation of Ras. *Neuron* **12**, 1207–1221 (1994).
19. Thomas, G.M. & Huganir, R.L. MAPK cascade signalling and synaptic plasticity. *Nat. Rev. Neurosci.* **5**, 173–183 (2004).
20. Itoh, M., Yamamoto, T., Nakajima, Y. & Hatta, K. Multistepped optogenetics connects neurons and behavior. *Curr. Biol.* **24**, R1155–R1156 (2014).
21. Dai, Y. *et al.* Phosphorylation of extracellular signal-regulated kinase in primary afferent neurons by noxious stimuli and its involvement in peripheral sensitization. *J. Neurosci.* **22**, 7737–7745 (2002).
22. Arrenberg, A.B. & Driever, W. Integrating anatomy and function for zebrafish circuit analysis. *Front. Neural Circuits* **7**, 74 (2013).
23. Ronneberger, O. *et al.* ViBE-Z: a framework for 3D virtual colocalization analysis in zebrafish larval brains. *Nat. Methods* **9**, 735–742 (2012).
24. Mueller, T. & Wullimann, M.F. *Atlas of Early Zebrafish Brain Development* (Elsevier, 2005).
25. Rohlfing, T. & Maurer, C.R. Nonrigid image registration in shared-memory multiprocessor environments with application to brains, breasts, and bees. *IEEE Trans. Inf. Technol. Biomed.* **7**, 16–25 (2003).
26. Jefferis, G.S.X.E. *et al.* Comprehensive maps of *Drosophila* higher olfactory centers: spatially segregated fruit and pheromone representation. *Cell* **128**, 1187–1203 (2007).
27. Portugues, R., Feierstein, C.E., Engert, F. & Orger, M.B. Whole-brain activity maps reveal stereotyped, distributed networks for visuomotor behavior. *Neuron* **81**, 1328–1343 (2014).
28. Orger, M.B., Kampff, A.R., Severi, K.E., Bollmann, J.H. & Engert, F. Control of visually guided behavior by distinct populations of spinal projection neurons. *Nat. Neurosci.* **11**, 327–333 (2008).
29. Huang, K.-H., Ahrens, M.B., Dunn, T.W. & Engert, F. Spinal projection neurons control turning behaviors in zebrafish. *Curr. Biol.* **23**, 1566–1573 (2013).
30. Pearson, G. *et al.* Mitogen-activated protein (MAP) kinase pathways: regulation and physiological functions. *Endocr. Rev.* **22**, 153–183 (2001).
31. Fernandes, A.M. *et al.* Deep brain photoreceptors control light-seeking behavior in zebrafish larvae. *Curr. Biol.* **22**, 2042–2047 (2012).
32. Satou, C. *et al.* Transgenic tools to characterize neuronal properties of discrete populations of zebrafish neurons. *Development* **140**, 3927–3931 (2013).
33. Tabor, K.M. *et al.* Direct activation of the Mauthner cell by electric field pulses drives ultra-rapid escape responses. *J. Neurophysiol.* **112**, 834–844 (2014).
34. Kimmel, C.B., Patterson, J. & Kimmel, R.O. The development and behavioral characteristics of the startle response in the zebra fish. *Dev. Psychobiol.* **7**, 47–60 (1974).
35. Prober, D.A. *et al.* Zebrafish TRPA1 channels are required for chemosensation but not for thermosensation or mechanosensory hair cell function. *J. Neurosci.* **28**, 10102–10110 (2008).
36. Amaral, D.G. & Sinnamon, H.M. The locus coeruleus: neurobiology of a central noradrenergic nucleus. *Prog. Neurobiol.* **9**, 147–196 (1977).
37. Lacoste, A.M.B. *et al.* A convergent and essential interneuron pathway for Mauthner-cell-mediated escapes. *Curr. Biol.* **25**, 1526–1534 (2015).
38. Bianco, I.H., Kampff, A.R. & Engert, F. Prey capture behavior evoked by simple visual stimuli in larval zebrafish. *Front. Syst. Neurosci.* **5**, 101 (2011).
39. Gahtan, E., Tanger, P. & Baier, H. Visual prey capture in larval zebrafish is controlled by identified reticulospinal neurons downstream of the tectum. *J. Neurosci.* **25**, 9294–9303 (2005).
40. Edwards, G.L. & Ritter, R.C. Ablation of the area postrema causes exaggerated consumption of preferred foods in the rat. *Brain Res.* **216**, 265–276 (1981).
41. van de Ven, V.G., Formisano, E., Prvulovic, D., Roeder, C.H. & Linden, D.E.J. Functional connectivity as revealed by spatial independent component analysis of fMRI measurements during rest. *Hum. Brain Mapp.* **22**, 165–178 (2004).
42. Freeman, J. *et al.* Mapping brain activity at scale with cluster computing. *Nat. Methods* **11**, 941–950 (2014).
43. McKeown, M.J. *et al.* Analysis of fMRI data by blind separation into independent spatial components. *Hum. Brain Mapp.* **6**, 160–188 (1998).
44. Hyvärinen, A. & Oja, E. Independent component analysis: algorithms and applications. *Neural Netw.* **13**, 411–430 (2000).
45. Dreosti, E., Llopis, N.V., Carl, M., Yaksi, E. & Wilson, S.W. Left-right asymmetry is required for the habenulae to respond to both visual and olfactory stimuli. *Curr. Biol.* **24**, 440–445 (2014).
46. Bianco, I.H. & Wilson, S.W. The habenular nuclei: a conserved asymmetric relay station in the vertebrate brain. *Phil. Trans. R. Soc. Lond. B* **364**, 1005–1020 (2009).
47. Wullimann, M.F., Rupp, B. & Reichert, H. *Neuroanatomy of the Zebrafish Brain*. (Birkhauser, 1996).
48. Liu, J. *et al.* Evolutionarily conserved regulation of hypocretin neuron specification by Lhx9. *Development* **142**, 1113–1124 (2015).
49. Wu, G.Y., Deisseroth, K. & Tsien, R.W. Spaced stimuli stabilize MAPK pathway activation and its effects on dendritic morphology. *Nat. Neurosci.* **4**, 151–158 (2001).
50. Ha, S. & Redmond, L. ERK mediates activity dependent neuronal complexity via sustained activity and CREB-mediated signaling. *Dev. Neurobiol.* **68**, 1565–1579 (2008).

ONLINE METHODS

Subjects. Zebrafish larvae were raised in E3 media supplemented with 1 mM HEPES buffer, pH 7.0. Larvae and adult fish were maintained on a 14-h:10-h light:dark cycle at 28 °C. All protocols and procedures involving zebrafish were approved by the Harvard University/Faculty of Arts & Sciences Standing Committee on the Use of Animals in Research and Teaching. For MAP-mapping experiments, the fish to be compared were usually all siblings from the same clutch, grown at a density of ~0.5 fish/mL, and distributed randomly into treatment groups. In the few cases where a single clutch did not yield sufficient numbers, two clutches were pooled and then distributed randomly so as to avoid any clutch-specific effects. Transgenic fish lines used in this study (**Supplementary Table 1**) have been described previously[2,32,37,48,51–64], with the exception of Tg(*elavl3*:H2B-RFP). For this transgenic construct, H2B-RFP was cloned downstream of an AttR1-R2 cassette flanked by Tol2 arms and then placed under the control of *elavl3* (HuC) *cis*-regulatory sequences via L-R recombination (Gateway cloning) with an AttL-flanked *elavl3* entry clone[2].

Immunohistochemistry. Because pERK is a fast indicator, fish need to be fixed as rapidly and consistently as possible across treatment groups. We quickly collected the fish by funneling the plate through a fine-mesh sieve and then immediately dropping the sieve into 4% paraformaldehyde (PFA) in PBS + 0.25% Triton (PBT). Fish were then immunostained using standard procedures. Briefly, fish were washed in PBT, incubated in 150 mM Tris-HCl, pH 9, for 15 min at 70 °C (ref. 65), washed in PBT, permeabilized in 0.05% Trypsin-EDTA for 45 min on ice, washed in PBT, blocked in PBT + 1% bovine serum albumin (BSA) + 2% normal goat serum (NGS) + 1% dimethyl sulfoxide (DMSO), and then incubated overnight at 4 °C in primary and secondary antibodies in PBT + 1% BSA + 1% DMSO. The pERK antibody (Cell Signaling, 4370) and tERK antibody (Cell Signaling, 4696) were used 1:500. Other primary antibodies and dilutions can be found in **Supplementary Table 1**. Secondary antibodies conjugated with Alexa fluorophores (Life Technologies) were diluted 1:500.

Confocal imaging. Imaging of stained tissue was done with an upright confocal microscope (Olympus FV1000, Zeiss LSM710 or Zeiss LSM780) using a 20×/1.0-NA (numerical aperture) water-dipping objective. Fish were mounted dorsal-side up in 2% (wt/vol) low-melting-point agarose (Invitrogen) and imaged at a voxel size of ~0.8 × 0.8 × 2 µm ($x \times y \times z$). To cover the entire brain, we acquired two imaging tiles and stitched them together using the Pairwise Stitching plugin in FIJI[66]. All fish to be analyzed in a MAP-mapping experiment were mounted together on a single imaging dish and imaged in one run to ensure that they were imaged with near-identical imaging conditions. Because all imaging was performed from the dorsal aspect, image intensity and quality were somewhat degraded in the more ventral regions of the brain.

Two-photon calcium imaging. For calcium imaging measurements and quantitative comparison with pERK levels (**Fig. 2d**,**e**), 6-dpf Tg(*elavl3*:GCaMP5G) larvae were anesthetized in MS-222 and mounted in 2% low-melting-point agarose, and an anatomy stack was acquired at 1 × 1 × 2 µm voxel size while the fish were under anesthesia. We removed the anesthetic and imaged the fish in a single plane at 2 Hz using a custom two-photon microscope[29,67] while presenting forward-moving gratings to activate neurons in the hindbrain. Regions of interest (ROIs) in the cell-body regions were generated using the watershed algorithm in Matlab. Activity within an ROI was detected as an event when the fluorescence Z-trace was above a threshold of 2, after application of a 1 × 5 moving-average filter in time. The total number of frames above the threshold was considered as the total time that neuron was active during imaging. After imaging, the fish were rapidly removed from the microscope, dissected out of the agarose and fixed in 4% PFA. After staining for pERK and tERK, we obtained confocal imaging stacks of the pERK level and the residual GCaMP5G expression. This GCaMP expression was used for registering the fixed data into the anatomy stack acquired live (**Supplementary Fig. 2**). The correlation between total firing time and pERK level in each ROI was calculated with Matlab's "corr" function. To visually highlight active neurons, we calculated the correlation between each pixel's time series and the summed signal of an approximately cell-sized (15 × 15 pixel) square surrounding that pixel (similarly to ref. 27) and overlayed it with the pERK level in the registered imaging plane. Calculations for the ROC analysis and the area under the curve were performed with Matlab's "roc" and "perfcurve" functions.

For neural-activity measurements related to routine turns triggered by leftward- or rightward-moving sinusoidal gratings (**Fig. 3d**), 6-dpf Tg(*elavl3*:GCaMP5G) larvae were paralyzed in α-bungarotoxin (1 mg/ml for ~60 s; Invitrogen) in E3 medium and embedded in 1.2% low-melting-point agarose (Invitrogen). Two-photon image stacks were acquired with an excitation pulsed Ti-sapphire laser tuned to 920 nm (Spectra Physics) while a flickering stimulus was projected from below with a digital light processing projector, which allowed simultaneous visual stimulation and detection of green fluorescence. In each experiment, images were acquired at 2.75 Hz, with a minimum of four repetitions per stimulus set and z-plane. We analyzed the resulting image time and depth series in Matlab to extract the positional origin of functional responses to leftward and rightward motion. We generated directional activity maps by dividing the average fluorescence change during stimulus presentation in one direction by the average fluorescence change in the opposite direction, at each voxel. Data from 17 fish imaged in the vicinity of the pretectum and anterior hindbrain (between 2 and 39 imaging planes per fish at 3-µm spacing) were registered to the Z-Brain. We combined the activity maps from all fish by calculating the average activity signal per pixel, and we smoothed them using the "Median_3D" filter in FIJI (x, y and z = 3, 3 and 2 pixels).

For tap and shock stimulation experiments (**Fig. 4h**), 6-dpf Tg(−6.7FR*hcrtR*:Gal4VP16); Tg(*uas*:GCaMP5G) larvae[37] were paralyzed in α-bungarotoxin and mounted in 2% low-melting-point agarose. Three repetitions of alternating tap and shock stimuli were given at 30-s intervals, repeated in z-planes to cover the majority of the hindbrain at 3-µm z-steps. We delivered taps by striking the imaging platform with a solenoid (Guardian Electric 28P-I-12D). Electric shocks were 100-ms pulses of 15 V delivered over a 6-cm dish, with the anode and cathode aligned to the head and tail of the fish, respectively, to maximize responses[33]. We created activity maps by correlating the signal in each voxel with a vector representing the stimulus delivery convolved with an

exponential-decay kernel approximating the GCaMP5G decay rate[68] (half-life = 0.667 s) and calculating the maximum-intensity Z projection over 17 imaging planes (51 µm).

ChR2 activation. Stimulated fish were 6-dpf Tg(−6.7FR*hcrtR*:Gal4VP16); Tg(14x*UAS-E1b*:hChR2(H134R)-EYFP); *atoh7*$^{th241/th241}$; Tg(*atoh7*:GAP-RFP)[37,69,70]. Blind *atoh7* mutant fish were used to prevent retinal-driven neural responses to light and were screened for a lack of retinal ganglion cells using the Tg(*atoh7*:GAP-RFP) label. Fish were first paralyzed with 1 µM bungarotoxin (Invitrogen) and anesthetized with MS-222 for 30 min to minimize background staining. Anesthetic solution was then washed away, and fish were stimulated for 5 min with either blue or green light from an arc lamp under a fluorescent dissecting scope, after which they were immediately fixed in 4% PFA.

Behavioral stimuli. *Light flash.* To adapt larvae to the dark, we covered their dishes with tinfoil-covered boxes for 3–4 h. Light stimuli were delivered for 10 s with a fluorescent light source suspended above the dish, yielding a light level of ~2,500 lx, and then fish were returned to darkness.

Optomotor stimuli. Fish were stimulated and recorded using a previously described apparatus[29]. The fish were stimulated for 5 min with sinusoidal light/dark gratings moving to either the right or the left. The stimulus was presented in a closed loop, such that the stimulus always moved in the same direction relative to the long axis of the fish. Fish were then quickly caught using a pipette and fixed in 4% PFA for MAP-mapping.

Aversive stimuli. In 85-mm petri dishes, fish were exposed to mustard oil (10 mM) or DMSO control (0.1%). For taps, the petri dish was placed on an acrylic platform in a dark box. After 30 min of dark-adaptation, the platform was struck with a solenoid (Guardian Electric 28P-I-12D) driven at 5 V using a Teensy 2.0 microcontroller (https://www.pjrc.com/teensy/), which produces short- and long-latency escape responses (data not shown). Taps were delivered every 10 s for 15 min. Controls were placed in the same dark box, but beside the tapping platform rather than on it, and were isolated from the tap stimuli. For heat stimulation, fish were put in 45 mL of E3 in 50-mL Falcon tubes and submerged in a 37 °C water bath for 15 min. The control Falcon tube was placed beside the water bath. Finally, for shock experiments, fish were placed in a 6-cm petri dish, over which a 100-ms, 15-V (2.5 V/cm) shock was delivered every 10 s for 15 min. Current was delivered using alligator clips and a previously described apparatus[71]. Controls were placed beside the shocked dish and were also affixed with alligator clips but were not connected to the circuit.

Feeding and hunting. An 85-mm petri dish containing the 6-dpf fish that had not previously been fed was inoculated with filtered paramecia. Fish were left to hunt and feed for 1 h (feeding was confirmed visually) and then were fixed in PFA. Controls were inoculated with water over the same time period.

Image registration. Nonrigid image registration was done with CMTK (http://www.nitrc.org/projects/cmtk/) and a user interface written by Jefferis and colleagues[72] with the command string (-awr 010203 -T 8 -X 52 -C 8 -G 80 -R 3 -A '--accuracy 0.4' -W '--accuracy 1.6'). This setup performed registrations at <15 min/fish on a 2 × 3.2 GHz Quad-Core Mac Pro (Apple). Our template brain was a 6-dpf *nacre* mutant (*mifta*$^{-/-}$) larvae[73] stained with anti-tERK. Staining the fish to be registered with anti-tERK allows for direct registrations to the template. However, in cases where a mouse IgG1-class primary antibody was used as a cell-type label, anti-tERK could not be used easily as a costain. In these cases we registered fish into the template brain indirectly by staining with anti-Syt2/Znp1 and using the anti-Znp1 mean stack as a template. To register the live two-photon calcium imaging data during right and left OMR stimulation (**Fig. 3d**), we used a single registered Tg(*elavl3*:GCaMP5G) fish as the template and the command string (-awr 010203 -T 2 -X 52 -C 8 -G 80 -R 4 -A '--accuracy 0.4' -W '--accuracy 0.8'). To register in the live-imaging two-photon data of Tg(*elavl3*:GCaMP5G) fish and the post-fixation data from the same fish to re-identify cells (**Supplementary Fig. 2**), we registered the GCaMP5G channel imaged by confocal microscopy after fixation into the anatomy stack taken live by two-photon microscopy using the command string (-awr 010203 -T 4 -X 200 -C 4 -G 160 -R 5 -A '--accuracy 0.4' -W '--accuracy 0.4').

Z-Brain creation. We created the mean-stack labels in the Z-Brain in Matlab by calculating the mean value across all registered fish stained with the given label and normalizing to the maximum-intensity value. Voxels that were not imaged in any given fish (for example, because of differential mounting or imaging coverage) were excluded from the mean calculation. These stacks were then integrated into a single HDF5 file, "AnatomyLabelDatabase.hdf5."

The Z-Brain regions were drawn manually using either the Segmentation Editor plugin in FIJI or our "ZBrainViewer.m" Matlab function, which utilizes the roipoly tool to draw 2D ROIs. In either case, 2D ROIs are drawn every ~3 *z*-planes to define the outline of a region. These ROIs are then interpolated in the *z*-dimension and smoothed by convolution with an ~8-µm-diameter sphere to create the 3D ROI volume defining an anatomical region. Regional mask definitions are contained in the file "MaskDatabase.mat." Finally, we also ranked all labels for their signal within each anatomical region, for both signal enrichment over the local surrounding area and mean signal within the region (**Supplementary Data 2**), providing a quantitative anatomical description of each region.

When segmenting the Z-Brain, we drew the regions at high resolution (maximally at cellular resolution). As a consequence, the Z-Brain contains extensive overlap between regions. This is in contrast to most neuroanatomical atlases, which contain exclusive boundaries (for example, http://www.virtualflybrain.org/ (*Drosophila*), http://atlas.brain-map.org/ (mouse) and refs. 23,24 (zebrafish)). Even in single brains there is clear overlap between groupings of neurons labeled by different markers (**Supplementary Fig. 1a**), and there is substantial biological noise in the position of some neuron types across brains. For these reasons, we felt that allowing for overlap would create a more accurate representation than would forcing hard borders. Ideally, a probabilistic approach to regional definition[74] should be developed for future versions of the Z-Brain, and for other high-resolution reference atlases. These segmentation efforts should also be computationally driven, rather than dependent on hand-drawn regions. This should be possible if the staining statistics are used across the many Z-Brain labels, and could even incorporate activity information through MAP-maps, calcium imaging and functional connectivity.

doi:10.1038/nmeth.3581

MAP-map calculation. Analysis was performed using FIJI/ImageJ[75] and Matlab (Mathworks). For MAP-map creation, post-warping pERK and/or tERK stacks are downsampled to resolutions in the *x*, *y* and *z* planes of 300, 679 and 80, respectively, and smoothed with a 2D Gaussian filter ($\sigma = 2$) using FIJI. This is done using the macro "PrepareStacksForMAPMapping.ijm." In Matlab, the Mann-Whitney *U*-statistic Z-score is calculated for each voxel, comparing between the two groups. The significance threshold is set using a false discovery rate (FDR)-based method, where 0.005% of control pixels would be called as significant. This is accomplished through the creation of a simulated control distribution of Z-scores using randomization of the voxel data into pseudogroups over 500 iterations and calculation of the FDR threshold value. If the absolute value of the treatment-versus-control Z-score is greater than this value, it is considered significantly different across the two groups, and the pixel is assigned an intensity equal to the difference in the median values of the groups (0:0.5 deta-median maps to 0:65535 intensity values). The voxel is color-coded according to its value (green denotes higher values and magenta denotes lower values in the treatment group). This analysis can be done with the "MakeTheMAPMap.m" Matlab function. For the projection images shown in the figures, the image lookup table was scaled linearly so that the saturation point was 60% of the maximum pixel intensity across the projection image. Unmanipulated MAP-maps were used for all quantitative analyses and can be downloaded from our website.

We calculated the intersection of aversive MAP-maps (**Fig. 4e**) by identifying which of the 4,928,427 brain voxels were significantly activated or suppressed across all four individual MAP-maps (**Fig. 4a–d**). The number of active voxels found was compared to chance levels of overlap using the χ^2 statistic (Matlab).

Analyzing MAP-maps with the Z-Brain atlas. To quantify the amount of MAP-map signal in the Z-Brain regions, we calculated the mean signal in each anatomical region and ranked the regions from highest to lowest average signal. This was done separately for the activation (positive) and suppression (negative) signals. In the regions that exhibited activity, we determined which Z-Brain label showed the most overlap with this signal by dividing the mean signal in the active voxels by the mean signal in the 50 voxels surrounding the region. Therefore, numbers greater than 1 indicated relative signal enrichment in the active voxels. The top five candidate cell-type labels were then listed, along with their enrichment signals. This analysis can be performed with the "ZBrainAnalysisOfMAPMaps.m" Matlab function.

Independent-component analysis. For ICA across fish, the registered tERK and pERK stack for each fish were downsampled to $x/y/z = 300/679/80$ resolution and smoothed with a 2D Gaussian filter ($\sigma = 2$), in the same way as is done for MAP-mapping. The central brain (not including eyes, ganglia or olfactory epithelia) from each fish was then downsampled into 4.7-μm^3 voxels, yielding a pERK-level vector for each fish. Fish in which any of the voxels was not imaged (as a result of incomplete coverage) were excluded from the analysis. We normalized fish for overall brightness by dividing by the tenth-percentile intensity value, and we normalized voxels by subtracting the mean value across fish. The fish-by-voxel array was then analyzed for spatially independent components using FastICA (http://research.ics.aalto.fi/ica/fastica/, Version 2.5), with each fish treated as a signal and each voxel treated as sample, using the symmetric approach, "pow3" nonlinearity, retaining the first 30 principal components and calculating 30 ICs. Spatial (rather than temporal) ICA was chosen for three reasons: (1) the relatively slow nature of the pERK-activity indicator, which will limit the temporal separation of signals; (2) the complex nature of the stimuli and experiences of the individual fish, which may not yield strictly temporally independent signals; and (3) the number of voxels, which dwarfs the number of observations (fish) in the data set[76]. IC maps are displayed as the Z-score values of the IC signals. Analyzed fish included those given no specific stimulus—both control fish from all MAP-maps presented here (**Figs. 2–4**) and additional fish treated with vehicle controls in other experiments not presented here—fish sampled throughout different points of the day and night and fish given one of various stimuli. This third group of additional fish included 'treatment' fish from all MAP-maps (**Figs. 2–5**) and other fish stimulated with electric shocks, light flashes, moving gratings, heat, mustard oil, melatonin, clonidine, nicotine, cocaine, ethanol and d-amphetamine.

Code access and supplementary software Instructions. The analysis code can be downloaded from the project website (http://engertlab.fas.harvard.edu/Z-Brain/). To report bugs and issues, please use the project github repository (https://github.com/owenrandlett/Z-Brain).

When running the Z-Brain viewer, ensure that the MaskDatabase.mat, AnatomyLabelDatabase.hdf5 and ZBrainViewer.m files are in a folder contained in your Matlab path, and then run the function "ZBrainViewer.m." Instructions on interacting with the data will be displayed on the screen.

Detailed instructions on the ZBrainViewer visualization options, as well as instructions on how to use the main MAP-map creating and analysis functions (MakeTheMAPMap.m and ZBrainAnalysisOfMAPMaps.m) are presented as headers of the functions.

51. Scott, E.K. *et al.* Targeting neural circuitry in zebrafish using GAL4 enhancer trapping. *Nat. Methods* **4**, 323–326 (2007).
52. Wen, L. *et al.* Visualization of monoaminergic neurons and neurotoxicity of MPTP in live transgenic zebrafish. *Dev. Biol.* **314**, 84–92 (2008).
53. McLean, D.L., Fan, J., Higashijima, S.-I., Hale, M.E. & Fetcho, J.R. A topographic map of recruitment in spinal cord. *Nature* **446**, 71–75 (2007).
54. Higashijima, S., Hotta, Y. & Okamoto, H. Visualization of cranial motor neurons in live transgenic zebrafish expressing green fluorescent protein under the control of the islet-1 promoter/enhancer. *J. Neurosci.* **20**, 206–218 (2000).
55. Ben Fredj, N.B. *et al.* Synaptic activity and activity-dependent competition regulates axon arbor maturation, growth arrest, and territory in the retinotectal projection. *J. Neurosci.* **30**, 10939–10951 (2010).
56. Shin, J., Park, H.-C., Topczewska, J.M., Mawdsley, D.J. & Appel, B. Neural cell fate analysis in zebrafish using olig2 BAC transgenics. *Methods Cell Sci.* **25**, 7–14 (2003).
57. Lambert, A.M., Bonkowsky, J.L. & Masino, M.A. The conserved dopaminergic diencephalospinal tract mediates vertebrate locomotor development in zebrafish larvae. *J. Neurosci.* **32**, 13488–13500 (2012).
58. Fujimoto, E., Stevenson, T.J., Chien, C.-B. & Bonkowsky, J.L. Developmental biology. *Dev. Biol.* **352**, 393–404 (2011).
59. Coffey, C.M. *et al.* Novel oxytocin gene expression in the hindbrain is induced by alcohol exposure: transgenic zebrafish enable visualization of sensitive neurons. *PLoS One* **8**, e53991 (2013).

60. Lillesaar, C., Stigloher, C., Tannhäuser, B., Wullimann, M.F. & Bally-Cuif, L. Axonal projections originating from raphe serotonergic neurons in the developing and adult zebrafish, *Danio rerio*, using transgenics to visualize raphe-specific pet1expression. *J. Comp. Neurol.* **512**, 158–182 (2009).
61. Parsons, M.J. *et al.* Notch-responsive cells initiate the secondary transition in larval zebrafish pancreas. *Mech. Dev.* **126**, 898–912 (2009).
62. Scott, E.K. & Baier, H. The cellular architecture of the larval zebrafish tectum, as revealed by gal4 enhancer trap lines. *Front. Neural Circuits* **3**, 13 (2009).
63. Kimmel, C.B., Powell, S.L. & Metcalfe, W.K. Brain neurons which project to the spinal cord in young larvae of the zebrafish. *J. Comp. Neurol.* **205**, 112–127 (1982).
64. Bae, Y.-K. *et al.* Developmental biology. *Dev. Biol.* **330**, 406–426 (2009).
65. Inoue, D. & Wittbrodt, J. One for all—a highly efficient and versatile method for fluorescent immunostaining in fish embryos. *PLoS One* **6**, e19713 (2011).
66. Preibisch, S., Saalfeld, S. & Tomancak, P. Globally optimal stitching of tiled 3D microscopic image acquisitions. *Bioinformatics* **25**, 1463–1465 (2009).
67. Ahrens, M.B. *et al.* Brain-wide neuronal dynamics during motor adaptation in zebrafish. *Nature* **485**, 471–477 (2012).
68. Chen, T.-W. *et al.* Ultrasensitive fluorescent proteins for imaging neuronal activity. *Nature* **499**, 295–300 (2013).
69. Zolessi, F.R., Poggi, L., Wilkinson, C.J., Chien, C.-B. & Harris, W.A. Polarization and orientation of retinal ganglion cells in vivo. *Neural Dev.* **1**, 2 (2006).
70. Kay, J.N., Finger-Baier, K.C., Roeser, T., Staub, W. & Baier, H. Retinal ganglion cell genesis requires lakritz, a zebrafish atonal homolog. *Neuron* **30**, 725–736 (2001).
71. Valente, A., Huang, K.H., Portugues, R. & Engert, F. Ontogeny of classical and operant learning behaviors in zebrafish. *Learn. Mem.* **19**, 170–177 (2012).
72. Ostrovsky, A., Cachero, S. & Jefferis, G. Clonal analysis of olfaction in *Drosophila*: image registration. *Cold Spring Harb. Protoc.* **2013**, 347–349 (2013).
73. Lister, J.A., Robertson, C.P., Lepage, T., Johnson, S.L. & Raible, D.W. nacre encodes a zebrafish microphthalmia-related protein that regulates neural-crest-derived pigment cell fate. *Development* **126**, 3757–3767 (1999).
74. Amunts, K., Schleicher, A. & Zilles, K. Cytoarchitecture of the cerebral cortex—more than localization. *Neuroimage* **37**, 1061–1065 (2007).
75. Schindelin, J. *et al.* Fiji: an open-source platform for biological-image analysis. *Nat. Methods* **9**, 676–682 (2012).
76. Calhoun, V.D., Adali, T., Pearlson, G.D. & Pekar, J.J. Spatial and temporal independent component analysis of functional MRI data containing a pair of task-related waveforms. *Hum. Brain Mapp.* **13**, 43–53 (2001).

doi:10.1038/nmeth.3581